**ATLAS NOTE**

ATLAS-CONF-2011-063

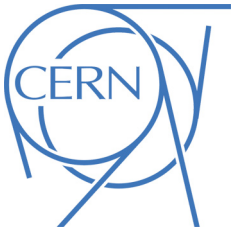

# Muon reconstruction efficiency in reprocessed 2010 LHC proton-proton collision data recorded with the ATLAS detector

The ATLAS collaboration

**Abstract**

This note presents measurements of the muon reconstruction and isolation efficiencies based on an analysis of $Z \to \mu^+\mu^-$ decays in an integrated luminosity of 40 pb$^{-1}$ of $\sqrt{s}$ = 7 TeV proton-proton collision data recorded with the ATLAS detector in 2010. The data entering the analysis were reprocessed with an optimized ATLAS reconstruction software and improved detector calibration and alignment.

# 1 Introduction

The ATLAS detector has been designed for efficient muon detection and high momentum resolution. The good relative momentum resolution of < 3.5% up to transverse momenta $p_{\mathrm{T}} \sim 200$ GeV and < 10% up to $p_{\mathrm{T}} \sim 1$ TeV is achieved by a combination of measurements from the inner detector and the muon spectrometer [1]. The complementarity of these measurements can be exploited to provide measurements of the muon reconstruction efficiencies in both of these tracking systems. In the present note, the muon reconstruction efficiencies are measured with $Z \rightarrow \mu^+\mu^-$ decays in which one of the decay muons is reconstructed in both systems and the other is identified by just one of the systems in order to probe the efficiency of the other. This so-called "tag-and-probe method" was successfully applied to the first pass reconstruction of the ATLAS proton-proton collision data recorded in 2010 at a centre-of-mass energy of 7 TeV [2]. The subject of this note is the muon reconstruction and muon isolation efficiency achieved after the reprocessing of the same data with optimized reconstruction software and improved detector calibration and alignment.

# 2 The ATLAS detector

A detailed description of the ATLAS detector can be found elsewhere [1]. Muons are independently measured in the inner detector (ID) and in the muon spectrometer (MS).

The ID measures tracks up to $|\eta| = 2.5$ [1] exploiting three types of detectors operated in a solenoidal magnetic field of 2 T: a silicon pixel detector closest to the interaction point, a silicon strip detector (SCT) surrounding the pixel detector, and a transition radiation straw tube tracker (TRT) covering $|\eta| < 2.0$ as the outermost part of the ID. The innermost layer of the pixel detector is referred to as the B-layer.

The MS consists of three large air-core superconducting toroidal magnet systems (two endcaps and one barrel) providing a field of approximately 0.5 T. The deflection of the muon trajectories in the magnetic field is measured via hits in three layers of precision drift tube (MDT) chambers for $|\eta| < 2$ and two layers of MDT chambers in combination with one layer of cathode strip chambers (CSC) in the innermost endcap wheels of the MS, for $2.0 \leq |\eta| < 2.7$. Three layers of resistive plate chambers (RPC) in the barrel ($|\eta| < 1.05$) and three layers of thin gap chambers (TGC) in the endcaps ($1.05 < |\eta| < 2.4$) provide the muon trigger and also measure the muon trajectory in the non-bending plane of the spectrometer magnets.

The ATLAS detector has a three-level trigger system: level 1 (L1), level 2 (L2), and the event filter (EF). The MS provides a L1 hardware muon trigger which is based on hit coincidences within different RPC or TGC detector layers inside programmed geometrical windows which define the muon $p_{\mathrm{T}}$. The L2 and EF muon triggers perform a software confirmation of the L1 muon trigger, by using refined $p_{\mathrm{T}}$ measurements from the precision chambers.

Figure 1 shows a schematic drawing of the ATLAS MS. The barrel muon chambers are installed in roughly cylindrical rings around the calorimeters. The endcap chambers are arranged in disks orthogonal to the proton beams. The BEE chambers are mounted on the endcap toroids. Large barrel chambers are mounted between the barrel toroid coils. Small barrel chambers are installed on and inside the toroid coils.

# 3 Detector map for muon efficiencies

As in [2], the efficiency is calculated as a function of the muon $p_{\mathrm{T}}$, $\eta$ and azimuthal angle, $\phi$. The available statistics was sufficient to measure the muon efficiency in eight transverse momentum bins

[1] $\eta = -\ln(\tan(\theta/2))$, where $\theta$ is the polar angle measured from the beam line.

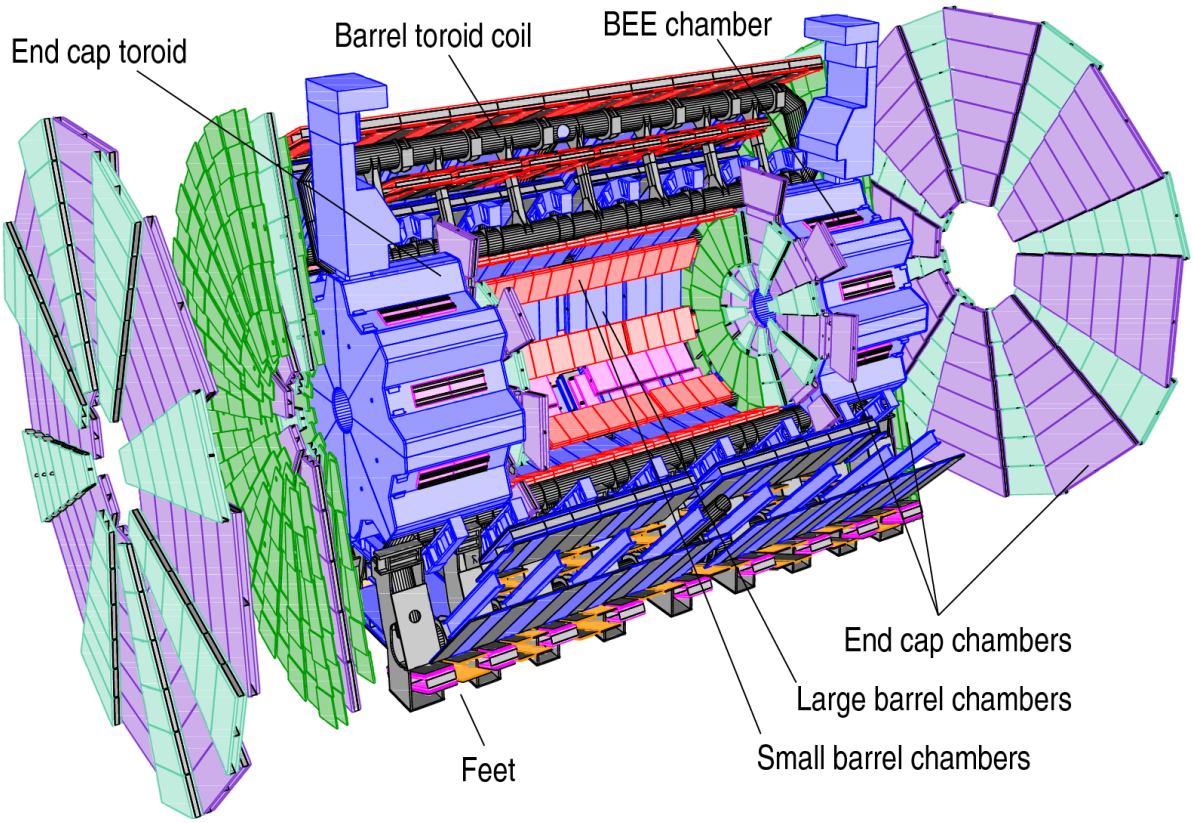


Figure 1: Schematic drawing of the ATLAS muon spectrometer

between 20 GeV and 100 GeV. The regions in $\eta - \phi$ space are grouped in a manner that follows the spectrometer configuration. Ten different regions are used, corresponding to ten different physical regions in the MS [1]. Figure 2 shows their locations in $\eta - \phi$ space. In each of these the muon will traverse a particular set of detector layers. The ten regions are labelled and described below:

- barrel large: large barrel stations;
- barrel small: small barrel stations;
- barrel overlap: overlap between small and large barrel stations;
- feet: region of the feet supporting the detector; some chambers are missing in this region which makes the muon reconstruction more difficult;
- transition: transition region between the barrel part and the endcap wheels;
- endcap small: small endcap sectors, MDT chambers;
- endcap large: large endcap sectors, MDT chambers;
- BEE: sectors containing barrel extended endcap chambers;
- CSC small: small endcap sectors, CSC chambers, outside TRT acceptance;
- CSC large: large endcap sectors, CSC chambers, outside TRT acceptance.

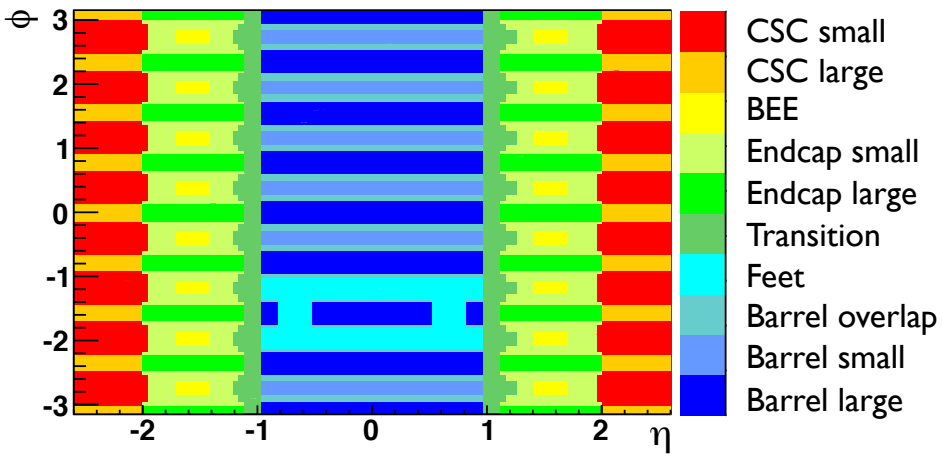


Figure 2: $\eta$-$\phi$ map of the coverage of the ten detector regions.

# 4 Muon identification in ATLAS

This note makes use of three classes of muons:

**Stand-alone (SA) muon:** The muon trajectory is only reconstructed in the MS. The direction of flight and the impact parameter of the muon at the interaction point are determined by extrapolating the spectrometer track back to the beam line taking the energy loss of the muon in the calorimeters into account;

**Combined (CB) muon:** Track reconstruction is performed independently in the ID and MS, and a track is formed from the successful combination of a MS track with an ID one;

**Segment tagged (ST) muon:** A track in the ID is identified as a muon if the track extrapolated to the MS is associated with straight track segments in the precision muon chambers.

The goal of the note is the measurement of the reconstruction efficiency for combined and segment tagged muons. Stand-alone muons are employed to measure the muon reconstruction efficiency in the inner detector as described in Section 5.

CB muons are the highest purity candidates. The efficiency for their reconstruction is determined mainly by the ability to form the independently reconstructed MS track, which varies with $\eta$ and $\phi$. This is most apparent in two regions:

- At $\eta \sim 0$ the MS is only partially equipped with muon chambers to provide space for services of the ID and the calorimeters.
- In the transition region between the barrel and the endcaps at $|\eta| \sim 1.2$ only one chamber is traversed by muons in the MS, due to staged endcap chambers. So no stand-alone momentum measurement is available and the CB muon efficiency is decreased.

The algorithms for ST muons have higher efficiency than those for CB muons as they can recover muons which did not cross enough precision chambers to allow an independent momentum measurement in the MS. They are also needed to reconstruct low $p_{\mathrm{T}}$ muons which only reach the inner layer of the muon chambers [3].

In the present early phase of the LHC operation ATLAS uses two algorithm chains for reconstructing ST and CB muons, namely chain 1 (Staco) and chain 2 (MuId). These follow different pattern recognition strategies and define the CB muon in slightly different ways [4] . In chain 1 it is required that the muon momentum is measured in both the ID and the MS. The momentum of the CB muon is then calculated as the weighted average of the ID and the MS stand-alone momentum measurements. The ID dominates the measurement up to $p_{\mathrm{T}} \sim 80$ GeV in the barrel and $p_{\mathrm{T}} \sim 20$ GeV in the endcaps. For higher $p_{\mathrm{T}} \lesssim 100$ GeV the ID and MS measurements have similar weight while the MS dominates at $p_{\mathrm{T}} \gtrsim 100$ GeV. In chain 2, instead of this statistical combination, a combined track fit to all muon hits in the ID and the MS is performed. The fit procedure includes recovery of missing or wrongly assigned spectrometer hits, most frequently arising from missing or low quality MS information in the transverse projection. A small fraction of combined muon tracks are formed from MS tracks without a momentum measurement (such as found in the transition region). When a muon is reconstructed as both a CB and ST muon, only the CB muon is used in the analysis.

### 4.1 Major changes to the first pass reconstruction software

The combined reconstruction algorithm of chain 1 has been improved compared to the version used in the first pass reconstruction in 2010. In that version, the association of stand-alone muons with inner detector tracks was performed by comparing the momentum of the stand-alone muon with the momentum of the inner detector track taking into account the corresponding uncertainties of the momentum measurements. As the estimate of the energy at the beam line for low-energy stand-alone muons has a large uncertainty due to the significant energy loss fluctuations of the muon in the calorimeters, the combination of a low-energy MS track with a high momentum ID track can satisfy the matching criteria. This incorrect association is avoided in the improved version of the chain 1 algorithm by also checking whether the inner detector track extrapolated into the MS can be geometrically matched with the MS track.

## 5 The tag-and-probe method

The reconstruction efficiency for CB or ST muons is the product of the muon reconstruction efficiency in the ID, the reconstruction efficiency in the MS, and the matching efficiency between the ID and MS measurements. Therefore it is possible to study the full reconstruction efficiency by measuring these individual efficiencies. The tag-and-probe method is sensitive to either the inner detector efficiency or the MS and matching efficiency.

In the tag-and-probe method, $Z \rightarrow \mu^{+}\mu^{-}$ decays are selected by requiring two oppositely charged isolated tracks with a dimuon invariant mass near the mass of the $Z$ boson. One of the tracks must be a CB muon. This track is called the *"tag muon"*. The other track, the so-called *"probe"*, must be a stand-alone muon if the ID efficiency is to be measured. If the MS and matching efficiency is to be measured the other track must be an inner detector track. The ID reconstruction efficiency is the fraction of stand-alone muon probes which can be associated to an inner detector track. The MS and matching efficiency is the fraction of ID probes which can be associated to a CB or ST muon. The impact of background events on the efficiency measurements is discussed in Section 6.6.

## 6 Selection of tag-and-probe pairs

The selection is performed in three steps: selection of collision events, tag selection and probe selection. These steps are discussed below. A detailed overview of the selection criteria is given in Table 1.

| Collision Event Selection | |
|---|---|
| Data quality | muon Good Runs List [3] |
| Primary vertex (PV) with ≥ 3 tracks | ≥ 1 |
| **ID Hit requirements** | |
| ID Si hit requirement | number of B layer hits > 0, pixel hits ≥ 2, SCT hits ≥ 6 |
| TRT hit requirements: $\|\eta\| \leq 1.9$ | Hits + Outliers > 5 & $\frac{\text{Outliers}}{\text{Hits+outliers}} < 0.9$ |
| TRT hit requirements: $\|\eta\| > 1.9$ | if (Hits + Outliers > 5): $\frac{\text{Outliers}}{\text{Hits+outliers}} < 0.9$ |
| **Tag Selection** | |
| Kinematics | $p_{\mathrm{T}} \geq 20$ GeV & $\|\eta\| \leq 2.4$ & $\|z_0\| < 10$ mm |
| Isolation | $\sum_{\text{tracks}} p_{\mathrm{T}}^{ID}/p_{\mathrm{T}} < 0.2$ tracks inside cone of 0.4 around tag |
| Trigger: | |
| Period A-D | $p_{\mathrm{T}} > 10$ GeV at level 1 |
| Period E-F | $p_{\mathrm{T}} > 10$ GeV at the event filter |
| Period G-I | $p_{\mathrm{T}} > 13$ GeV at the event filter |
| **Probe Selection** | |
| Kinematics | $p_{\mathrm{T}} \geq 20$ GeV & $\|\eta\| \leq 2.5$ & $\|z_0\| < 10$ mm |
| Isolation | $\sum_{\text{tracks}} p_{\mathrm{T}}^{ID}/p_{\mathrm{T}} < 0.2$ tracks inside cone of 0.4 around probe |
| Charge | Opposite charges of tag and probe |
| $\Delta\phi$(Tag,Probe) | > 2.0 |
| Invariant mass | $\|m_{\mathrm{Z}} - m_{\mathrm{TP}}\| < 10$ GeV |
| same vertex as Probe | $\|z_{0_{\mathrm{Tag}}} - z_{0_{\mathrm{Probe}}}\| < 3$ mm |
| **Probe - Muon matching** | |
| $\Delta R$ | < 0.01 |
| Charge | same |

Table 1: All cuts used to select the tag and probe pairs and to match probes to muons are summarized. The ID hit requirements are restricted to the instrumented areas; dead or missing sensors crossed by a track are counted as hits.

### 6.1 Collision event selection

The ID and MS, including their magnet systems, have to be fully operational for an event to be included in the analysis. Events must pass the lowest $p_{\mathrm{T}}$ threshold muon trigger that was unprescaled. The thresholds of the selected triggers ranged from 10 to 13 GeV and were well below the transverse momentum threshold of the tag muon in the analysis. To include only proton-proton collision events, a reconstructed primary vertex with at least three associated tracks is required.

### 6.2 Inner detector track selection

All tracks considered in the analysis must have a minimum number of hits in the silicon detectors. Dead or missing sensors crossed by a track are counted as hits. Within the geometrical acceptance of the TRT a successful extension of the muon trajectory into that detector is enforced by requirements on the numbers of associated good TRT hits and TRT outliers. TRT outliers appear in two forms in the track reconstruction, as a straw tube with a signal but not crossed by the near-by track or as a set of TRT measurements in the prolongation of a track which, however, failed to form a smooth trajectory together with the pixel and SCT measurements. These quality cuts are put in place to suppress fake tracks and

discriminate against muons from hadron decays. Combined and segment-tagged muons which do not fulfil the ID hits requirements are rejected in the analysis.

### 6.3 Tag selection

Tag muons are defined as combined muons from the primary vertex, separately for each of the two reconstruction chains. A combined muon has to pass the following cuts:

- the ID track on which the combined muon is based has to fulfil the track hit cuts listed in Table 1;
- $p_{\mathrm{T}} \geq 20$ GeV;
- $|\eta| \leq 2.4$, limited to the acceptance of the muon trigger system;
- longitudinal distance from primary vertex $|z_0| < 10$ mm;
- the tag muon must have triggered the data acquisition;
- isolation: $\sum p_{\mathrm{T}}(\Delta R < 0.4)/p_{\mathrm{T}}(\mathrm{tag}) < 0.2$ (with $\Delta R := \sqrt{\Delta\eta^2 + \Delta\phi^2}$), where the sum extends over all tracks within a cone of 0.4 around the tag, excluding the track on which the tag is based.

### 6.4 Probe selection

Probes are either stand-alone muons or inner detector tracks depending on which efficiency measurement is being performed. They have to pass the following criteria :

- ID probes must fulfil the ID track hit criteria listed in Table 1;
- $p_{\mathrm{T}} > 20$ GeV;
- $|\eta| < 2.5$, limited to the coverage of the ID;
- longitudinal distance from primary vertex $|z_0| < 10$ mm;
- isolation: $\sum p_{\mathrm{T}}(\Delta R < 0.4)/p_{\mathrm{T}}(\mathrm{probe}) < 0.2$, where the sum extends over all tracks within a cone of 0.4 around the probe, excluding the probe itself;
- the tag and the probe must be associated to the same vertex;
- azimuthal separation of tag and probe tracks, $\Delta\phi > 2.0$;
- the invariant mass of the tag-and-probe pair is close to the nominal $Z$ mass: $|m_{\mathrm{Z}} - m_{\mathrm{TP}}| < 10$ GeV;
- the tag and the probe are oppositely charged.

The additional quality requirements used in [2] to reject bad matches of stand-alone muons with inner detector tracks in chain 1 are no longer needed in the improved version of that combined reconstruction algorithm.

### 6.5 Probe - muon matching

After selecting all tag-and-probe pairs an attempt is made to match the probe tracks to muons in the event. A match between an ID probe and a muon is considered successful if they have the same measured charge and are close in $\eta-\phi$ space: $\Delta R \leq 0.01$. A match between a SA muon probe and an ID track is considered successful if $\Delta R \leq 0.05$.

### 6.6 Purity of the selected sample

According to Monte Carlo studies, 99.3% of the selected events with an inner detector probe contain dimuon decays of $Z$ bosons; the background events are $Z \to \tau^+\tau^-$, $W^\pm \to \mu^\pm(\bar{\nu}_\mu)$, $W^\pm \to \tau^\pm(\bar{\nu}_\tau)$, $b\bar{b}$, $c\bar{c}$, and $t\bar{t}$ as shown in [2]. The presence of background events leads to an apparently lower measured muon efficiency. This is visible in the plots of Figure 3 which, for CB muons using ID probes, shows the effect of the backgrounds on the measured efficiency in bins of detector region, $p_{\mathrm{T}}$, and $\eta$. Figures 3(c) and (d) show that the background mainly contributes to the region of low transverse momenta of the probe muons and is negligible for $p_{\mathrm{T}} \gtrsim 30$ GeV. The background contamination is below 0.1% for selected events with a stand-alone muon probe.

## 7 Measured muon reconstruction efficiencies

### 7.1 Inner detector reconstruction efficiency

As discussed earlier, and illustrated in Figure 3, the efficiency for the combined muon reconstruction varies with the detector region, and with $p_{\mathrm{T}}$ in the range below 6 GeV [5]. In contrast, the ID muon efficiency is independent of $\phi$ and $p_{\mathrm{T}}$[1]. It shows a small $\eta$ dependence as illustrated in Figure 4. The small efficiency drops at $\eta \sim 0$ and $\eta \sim 1$ are caused by the ID hit requirements listed in Table 1. At $\eta \sim 0$ ID tracks which pass through the dead region near the middle of the TRT barrel straws produce no TRT hits. At $|\eta| \sim 1$ there is a small region in the transition between the barrel and endcaps of the ID in which muons cross less than 6 SCT sensors. The measured ID muon reconstruction efficiency agrees with the Monte-Carlo prediction within the statistical errors of less than 1%. The measured ID efficiency is (0.991±0.001) on average due to the hit requirements imposed on the ID muon tracks. The results are independent of the choice of the algorithm chain for the stand-alone muon.

### 7.2 Combined muon reconstruction efficiency

Figure 5 shows the efficiency for CB muons as a function of $p_{\mathrm{T}}$, the detector region, and $\eta$ for data and simulation, relative to the ID efficiency. The simulation includes all considered backgrounds. The scale factor, defined as the ratio between data and Monte Carlo, is displayed in the lower panel of each plot. The mean value of the $\eta$ dependent scale factor curve is 0.989 ± 0.003 for chain 1 and 0.995 ± 0.002 for chain 2, where the errors are statistical. The 1% deviation from 1 in overall efficiency scale factor of chain 1 is caused by the efficiency scale factor of 0.94 in the transition region. The efficiency drop in the transition region is attributed to the limited accuracy of the magnetic field map used in the reconstruction of the ATLAS data in this region which leads to a small mismeasurement of the stand-alone muon momentum. The efficiency drops can be recovered by using muons which are tagged by only one muon station as described in detail below.

The scale factors determined in bins of $p_{\mathrm{T}}$ agree, within 1.5 standard deviations, with the average scale factor for the algorithm in question.

The background-corrected efficiencies for CB muons are shown in Figure 6. The background is estimated from Monte Carlo simulation, as described in Section 6.6. It is subtracted for every bin individually. The average CB muon reconstruction efficiency is 0.928 ± 0.002 for chain 1 and 0.958 ± 0.001 for chain 2. The difference in efficiency between the two chains arises mainly from more stringent requirements on the recontructed MS tracks considered for identifying a muon as combined muon in chain 1.

### 7.3 Efficiencies for combined plus segment tagged muons.

The degree to which some muon efficiency, in detector regions with partial muon coverage, can be recovered using segment tagging, has been studied by measuring the efficiency for CB plus ST muons. The same tag-and-probe method is used with the only difference that the probe is matched to a CB or ST muon. Figure 7 shows the measured combined plus segment tagged muon efficiencies as functions of the detector region, $p_{\mathrm{T}}$, and $\eta$, in comparison with the combined muon efficiencies. The gain in efficiency when using ST muons in addition to the CB muons is presented in the lower panels of the plots. These are largest in the ATLAS feet (13 %) and transition (15%) regions of the detector for chain 1. For the chain 2 algorithm the largest gain is 3 % in the feet and BEE regions. Figures 7(c) and (d) show that the two chains have similar overall efficiencies for combined plus segment tagged muons, 0.970±0.001 for chain 1 and 0.980±0.001 for chain 2.

In Figure 8 the efficiency for CB plus ST muons measured from data is compared to the Monte Carlo expectations and scale factors are derived. Remarkable agreement between the measured and predicted efficiencies is achieved. The scale factors for CB plus ST muons are 1.003±0.002 for chain 1 and 1.001±0.002 for chain 2.

## 8 Measurement of the muon isolation efficiency

A powerful tool for rejecting muons from hadron decays in the tag-and-probe efficiency measurement is isolation. It is therefore desirable to quantify the reliability of the Monte-Carlo prediction of the isolation efficiency. This is studied using the same event selection as was used for the efficiency measurements, up to the selection of the tag muon. In this case, the probe muon is defined as an isolated CB muon with $p_{\mathrm{T}} > 20$ GeV that fulfils the ID hit requirements of Table 1. We consider track isolation and calorimeter isolation:

- Track isolation: $\sum p_{\mathrm{T}}(\Delta R < 0.4(0.3))/p_{\mathrm{T}}(\mu)) < 0.2$ or 0.1, where the sum extends over all charged particle tracks within a cone of 0.4(0.3) around the probe, excluding the probe itself;
- Calorimeter isolation: the transverse energy deposition in the calorimeter ($E_{\mathrm{T}}$) in a cone of size $\Delta R < 0.4(0.3)$ around the muon is less than $0.2p_{\mathrm{T}}(\mu)$ or $0.1p_{\mathrm{T}}(\mu)$. The calorimeter isolation energy is corrected for the muon energy loss.

Figure 9 compares the distributions of the measured isolation variables for the probe muons with the Monte-Carlo prediction. The excellent agreement between the experimental and simulated distributions leads to a reliable prediction of the isolation efficiency which is defined as the fraction of probe muons passing a given set of isolation cuts. The measured isolation efficiencies and the corresponding Monte Carlo predictions are compared for chain 1 in Figure 10; the results for chain 2 are consistent. Experimental and simulated data agree within errors. The isolation efficiency in the $Z \to \mu^+\mu^-$ selection under study is well modelled by the ATLAS Monte Carlo simulation. The efficiency drops at low $p_{\mathrm{T}}(\mu)$ are mainly caused by the fact that the track $p_{\mathrm{T}}$ sums and $E_{\mathrm{T}}$, which depend only weekly on $p_{\mathrm{T}}(\mu)$, are divided by $p_{\mathrm{T}}(\mu)$, leading to isolation variables that rise with decreasing $p_{\mathrm{T}}(\mu)$. They are also partially due to the background which populates the low $p_{\mathrm{T}}(\mu)$ region.

## 9 Summary

The muon reconstruction and isolation efficiency has been studied with $Z \to \mu^+\mu^-$ decays for an integrated luminosity of 40 pb$^{-1}$ of proton-proton collision data recorded with the ATLAS detector in 2010.

The muon reconstruction efficiency is measured to be > 96% and agrees with the Monte-Carlo prediction to within less than 1%. The measurement of the isolation efficiency is in excellent agreement with the Monte-Carlo prediction.

# References


[1] ATLAS Collaboration, *The Atlas Experiment at the CERN Large Hadron Collider*, JINST **3** (2008) S08003.

[2] ATLAS Collaboration, *Determination of the muon reconstruction efficiency in ATLAS at the Z resonance in proton-proton collisions at* $\sqrt{s}$*=7 TeV*, ATLAS-CONF-2011-008, CERN, Geneva, 2011.

[3] ATLAS Collaboration, *Muon Reconstruction Performance*, ATLAS-CONF-2010-064, CERN, Geneva, 2010.

[4] ATLAS Collaboration, *Muon Performance in Minimum Bias pp Collision Data at* $\sqrt{s}$ = 7 *TeV with ATLAS*, ATLAS-CONF-2010-036, CERN, Geneva, 2010.

[5] ATLAS Collaboration, *A measurement of the ATLAS muon efficiency using* $J/\psi$ *decays*, ATLAS-CONF-2011-021, CERN, Geneva, 2011.

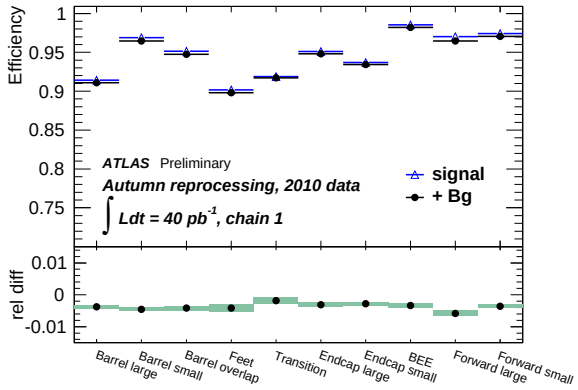


(a) Chain 1 efficiency for the different detector regions

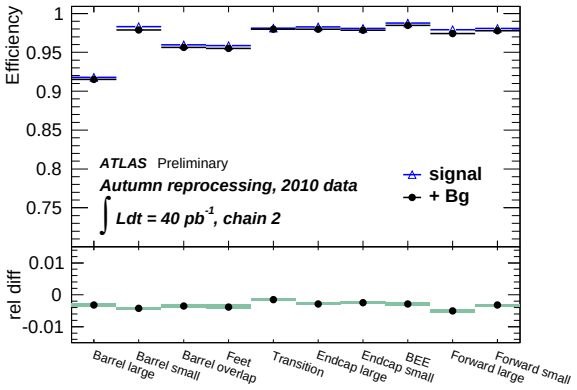


(b) Chain 2 efficiency for the different detector regions

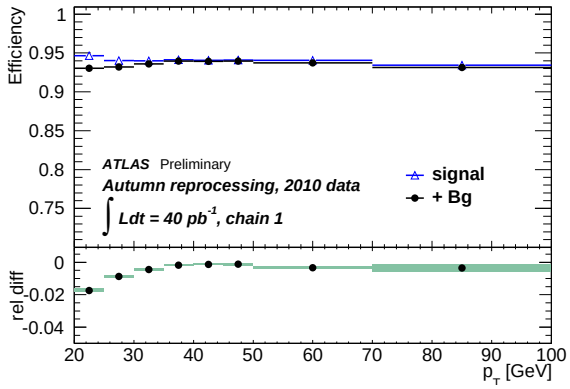


(c) Chain 1 efficiency as a function of muon $p_{\mathrm{T}}$

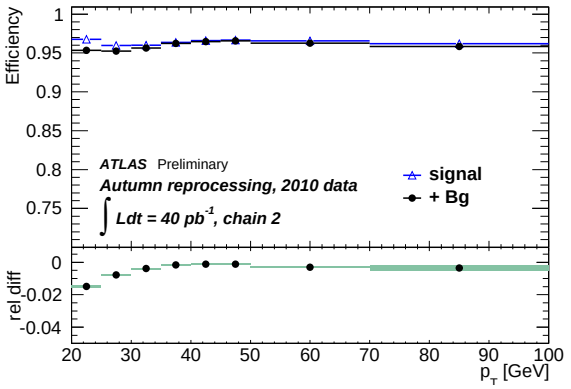


(d) Chain 2 efficiency as a function of the muon $p_{\mathrm{T}}$

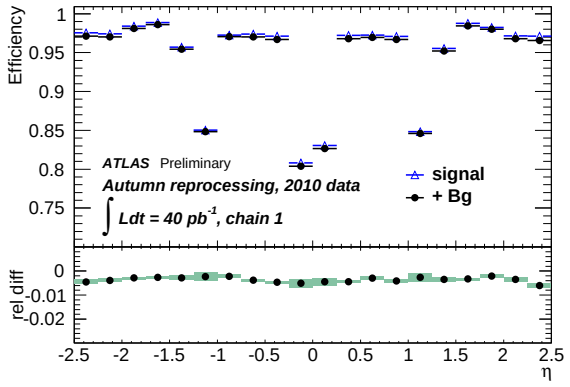


(e) Chain 1 efficiency as a function of muon $\eta$

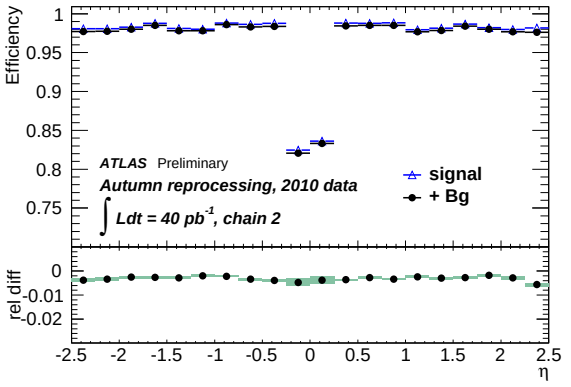


(f) Chain 2 efficiency as a function of the muon $\eta$

Figure 3: Measured efficiencies for combined muons from Monte Carlo simulated data for chain 1 and chain 2 using ID probes. The triangles correspond to efficiencies determined from the $Z \rightarrow \mu^{+}\mu^{-}$ sample only, while the black dots show the efficiencies obtained with the tag-and-probe method when backgrounds are included.

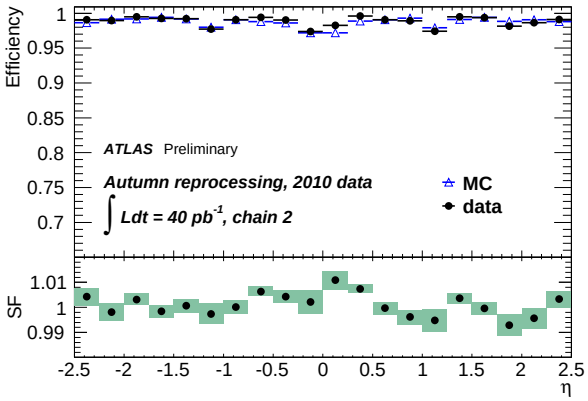


Figure 4: Comparison of the measured ID muon reconstruction efficiency as a function of $\eta$ with the Monte-Carlo prediction. The scale factors, defined as the ratios of the measured and the predicted efficiencies, are consistent with unity to within the uncertainties, which are less than about 1%. The inefficiencies are created by the hit requirements imposed on the ID tracks.

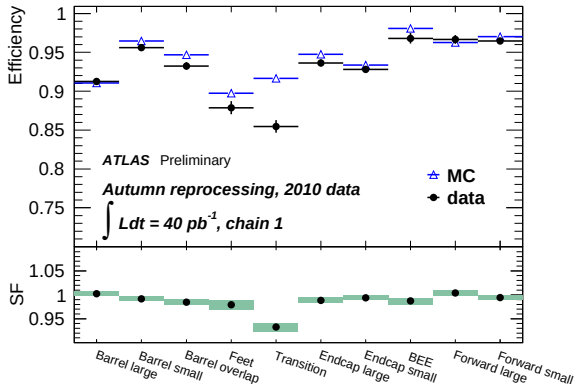


(a) Chain 1 efficiency for the different detector regions

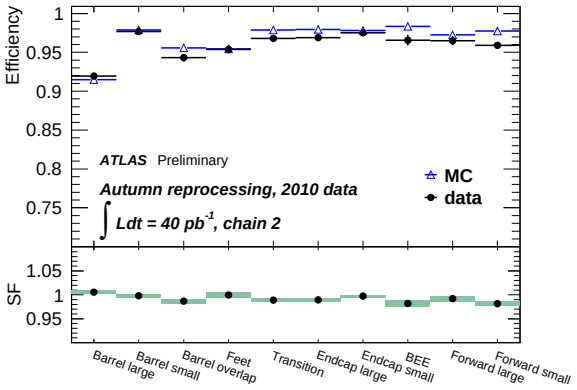


(b) Chain 2 efficiency for the different detector regions

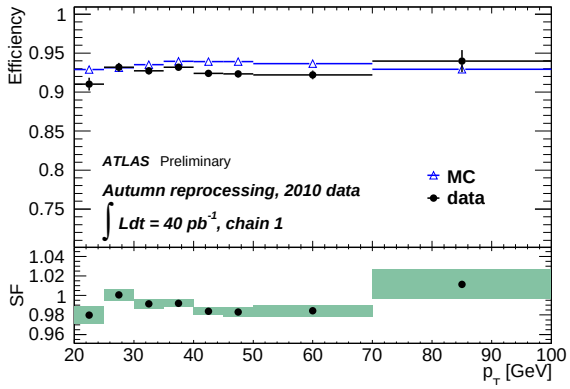


(c) Chain 1 efficiency as a function of muon $p_{\mathrm{T}}$

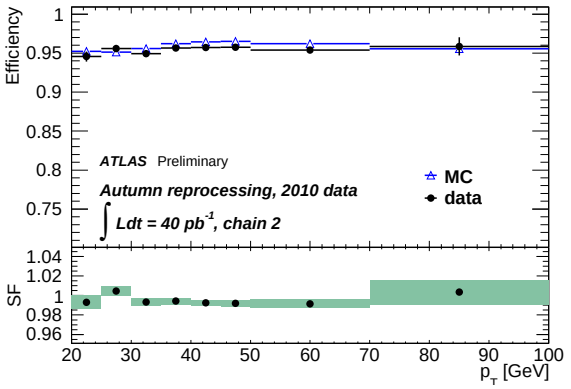


(d) Chain 2 efficiency as a function of muon $p_{\mathrm{T}}$

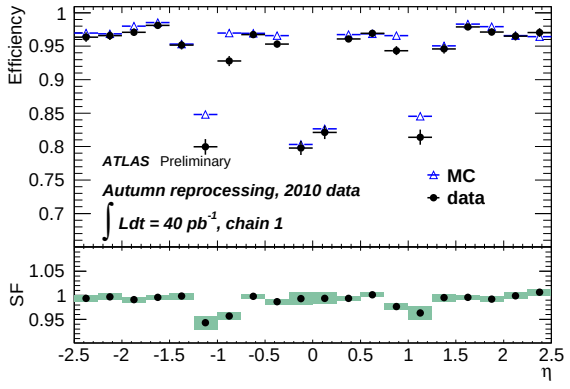


(e) Chain 1 efficiency as a function of muon $\eta$

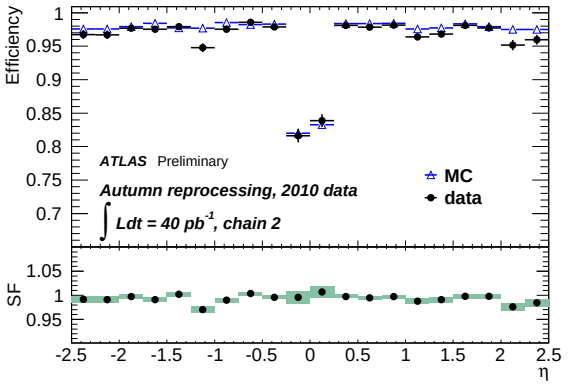


(f) Chain 2 efficiency as a function of muon $\eta$

Figure 5: Reconstruction efficiencies and scale factors for CB muons. The efficiencies for the two reconstruction chains, obtained from data (dots) without background correction and Monte Carlo simulation (open triangles) including backgrounds, are shown in the upper part of each figure. The corresponding scale factors are shown in the lower part.

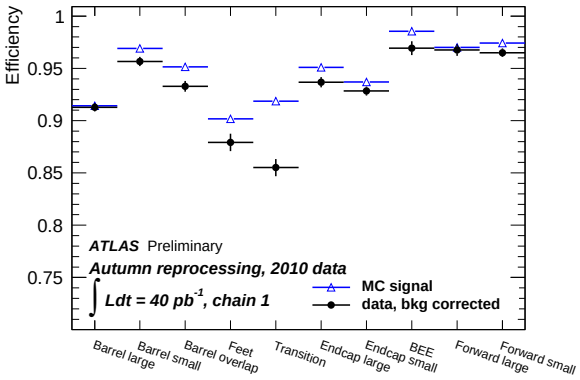


(a) Chain 1 efficiency for the different detector regions

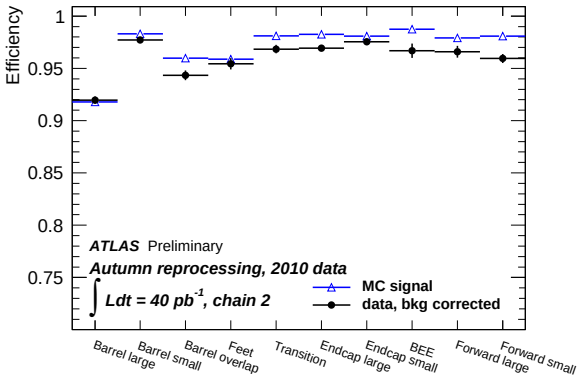


(b) Chain 2 efficiency for the different detector regions

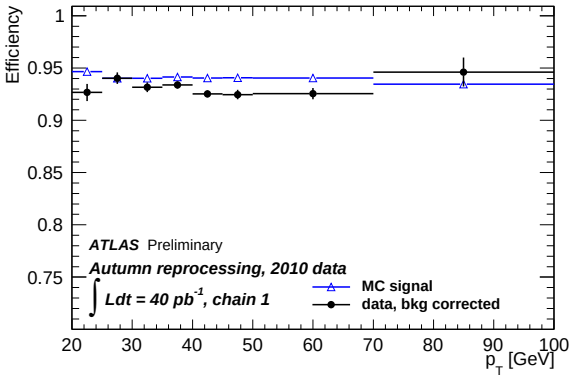


(c) Chain 1 efficiency as a function of muon $p_{\mathrm{T}}$

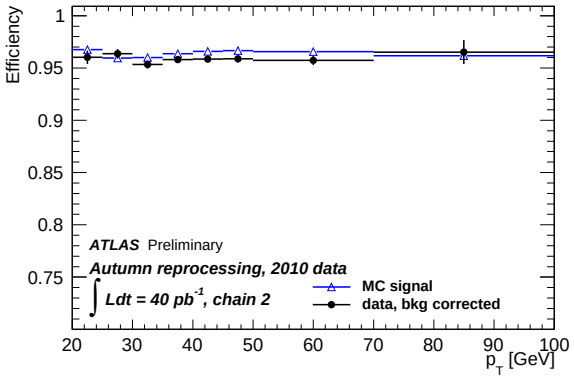


(d) Chain 2 efficiency as a function of muon $p_{\mathrm{T}}$

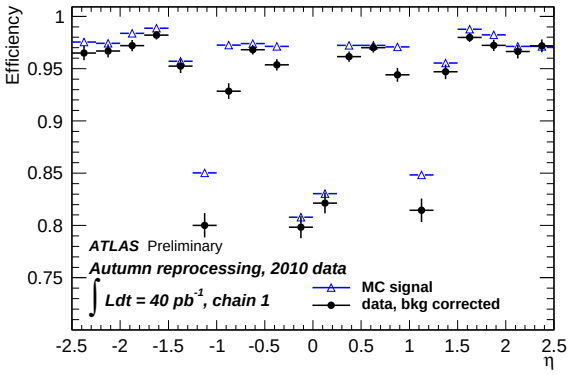


(e) Chain 1 efficiency as a function of muon $\eta$

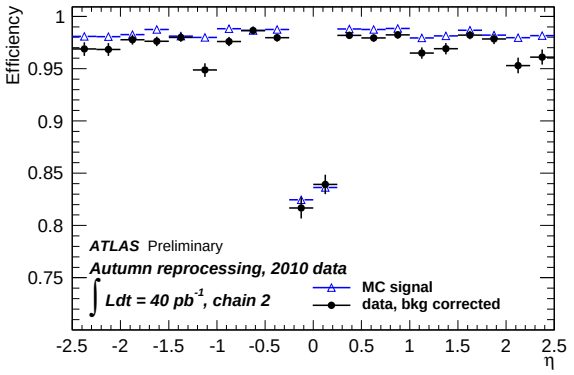


(f) Chain 2 efficiency as a function of muon $\eta$

Figure 6: Background corrected efficiencies for CB muons for the two reconstruction chains, obtained from data (dots) and Monte Carlo simulation (open triangles).

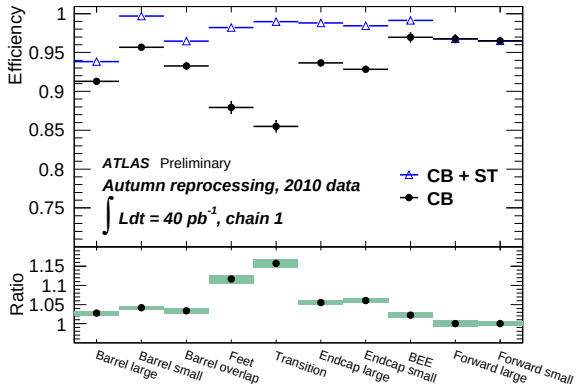


(a) Chain 1 efficiency for the different detector regions

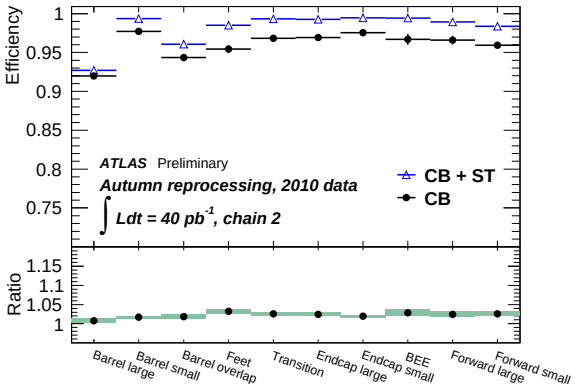


(b) Chain 2 efficiency for the different detector regions

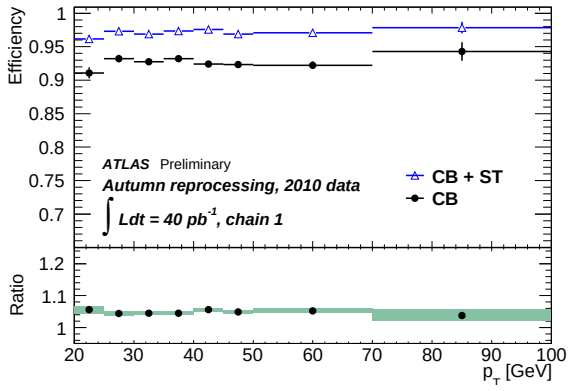


(c) Chain 1 efficiency as a function of muon $p_{\mathrm{T}}$

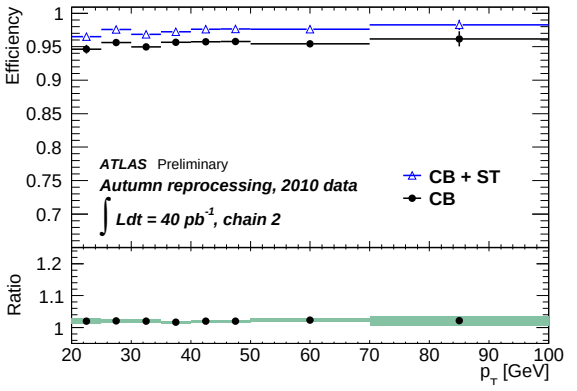


(d) Chain 2 efficiency as a function of muon $p_{\mathrm{T}}$

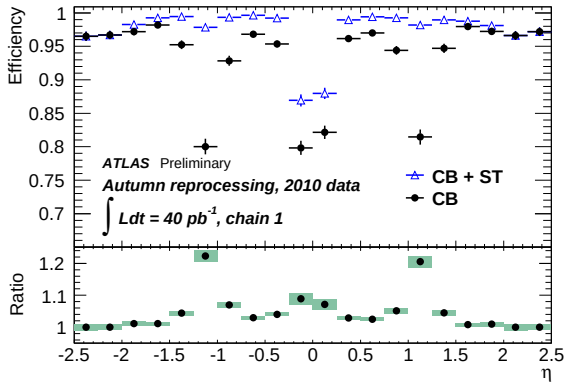


(e) Chain 1 efficiency as a function of muon $\eta$

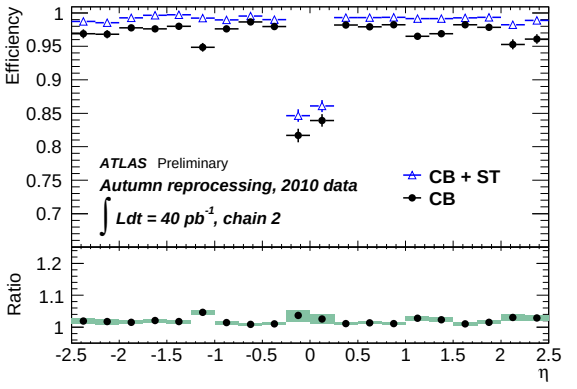


(f) Chain 2 efficiency as a function of muon $\eta$

Figure 7: Efficiencies for CB plus ST muons (open circles) in comparison to those for CB muons only (dots). The relative gain is shown in the lower part of each figure.

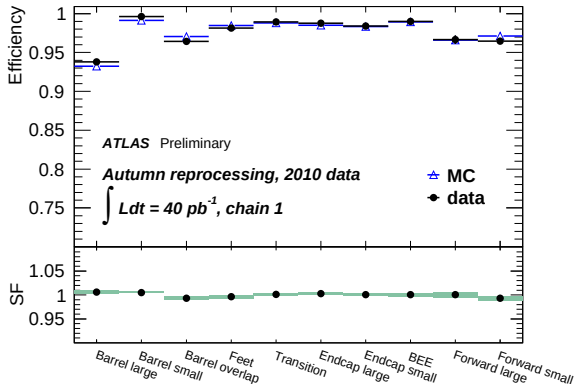


(a) Chain 1 efficiency for the different detector regions

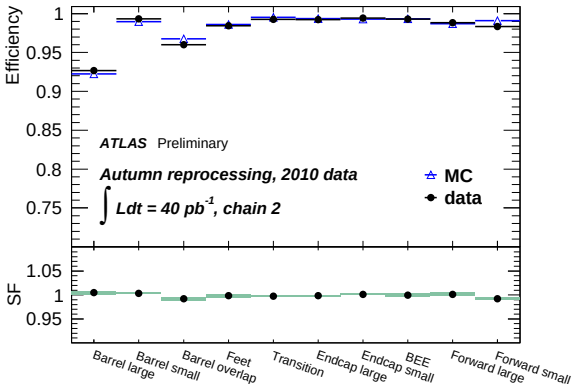


(b) Chain 2 efficiency for the different detector regions

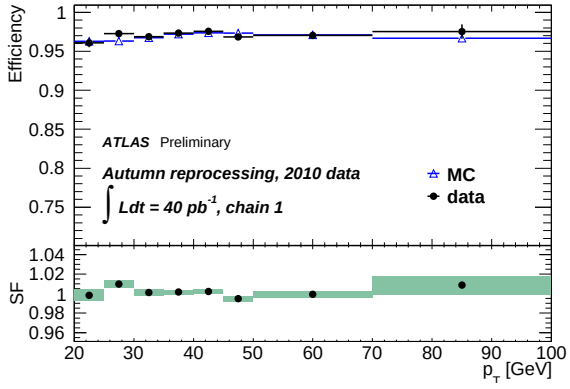


(c) Chain 1 efficiency as a function of muon $p_{\mathrm{T}}$

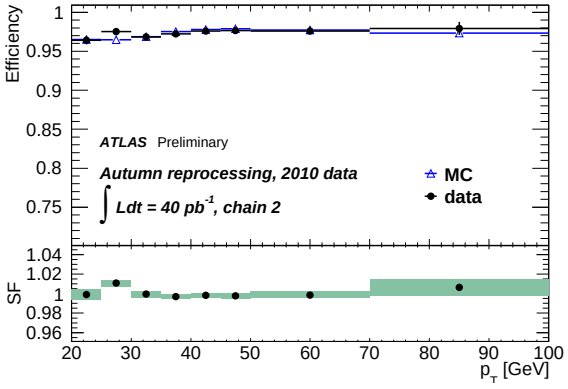


(d) Chain 2 efficiency as a function of muon $p_{\mathrm{T}}$

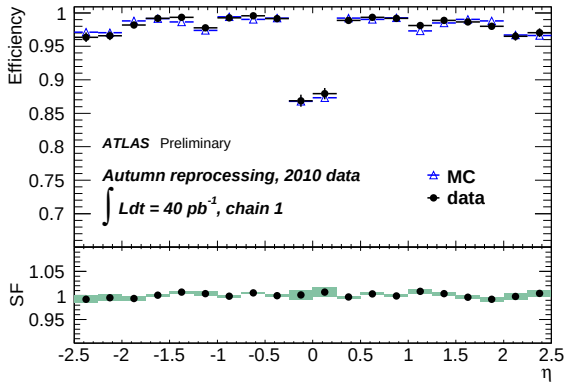


(e) Chain 1 efficiency as a function of muon $\eta$

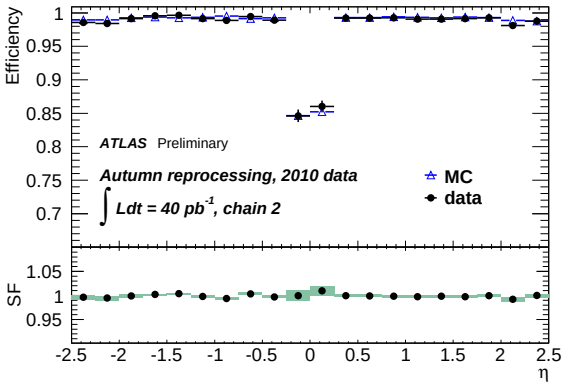


(f) Chain 2 efficiency as a function of muon $\eta$

Figure 8: Efficiencies for CB plus ST muons, obtained from data with background correction (dots) and Monte Carlo simulation of the signal (open triangles).

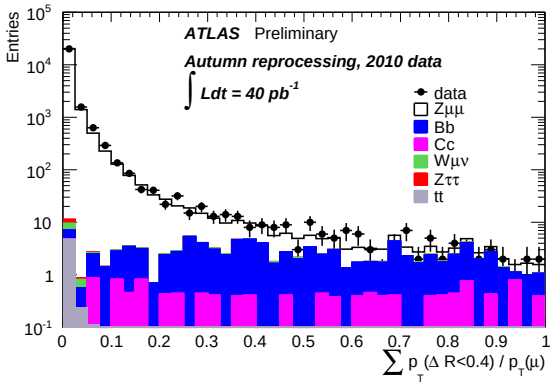


(a) Track isolation $\sum p_{\mathrm{T}}(\Delta R < 0.4)/p_{\mathrm{T}}(\mu)$

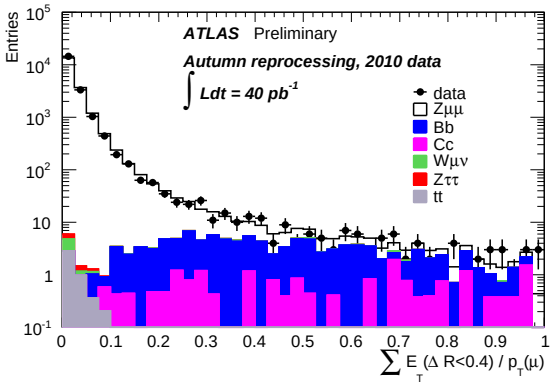


(b) Calorimeter isolation $E_{\mathrm{T}}(\Delta R < 0.4)/p_{\mathrm{T}}(\mu)$

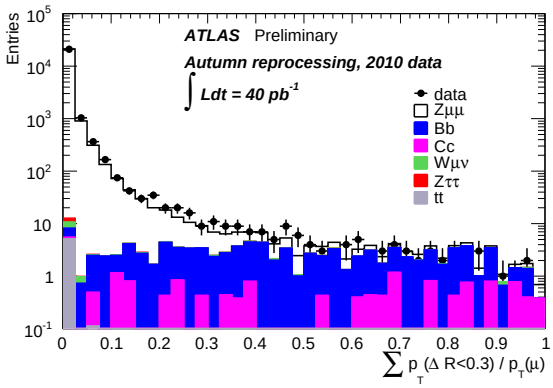


(c) Track isolation $\sum p_{\mathrm{T}}(\Delta R < 0.3)/p_{\mathrm{T}}(\mu)$

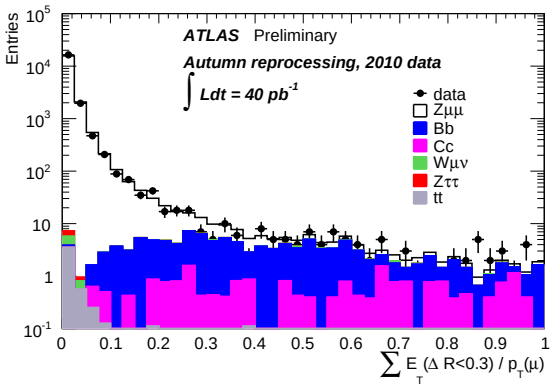


(d) Calorimeter isolation $E_{\mathrm{T}}(\Delta R < 0.3)/p_{\mathrm{T}}(\mu)$

Figure 9: Comparison of the measured track and calorimeter isolation distributions of the probe muon with the Monte-Carlo prediction for two different cone sizes.

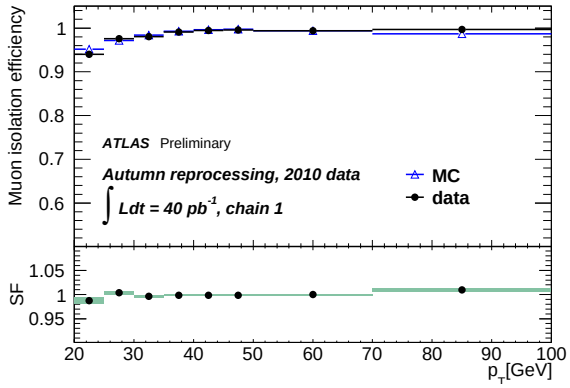


(a) Track isol. eff. for $\sum p_{\mathrm{T}}(\Delta R < 0.4)/p_{\mathrm{T}}(\mu) < 0.2$

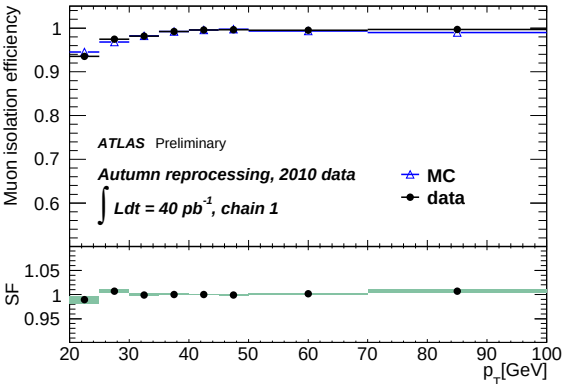


(b) Calorimeter isol. eff. for $E_{\mathrm{T}}(\Delta R < 0.4)/p_{\mathrm{T}}(\mu) < 0.2$

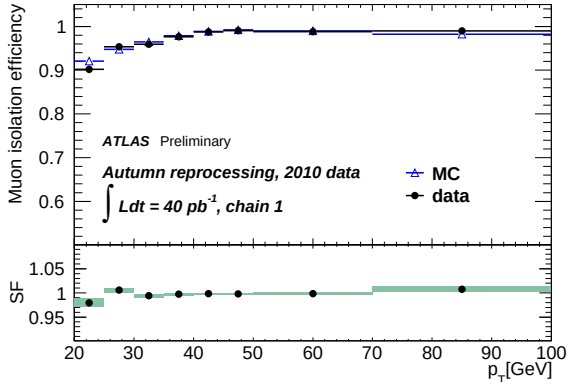


(c) Track isol. eff. for $\sum p_{\mathrm{T}}(\Delta R < 0.4)/p_{\mathrm{T}}(\mu) < 0.1$

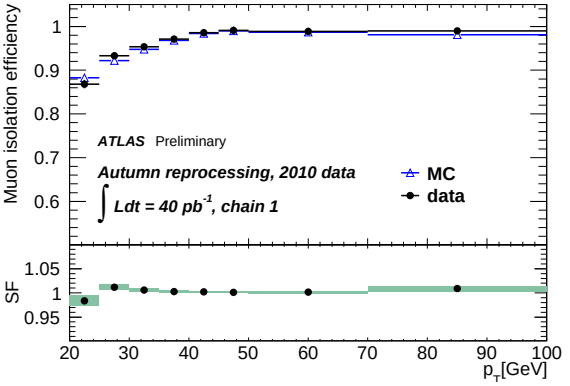


(d) Calorimeter isol. eff. for $E_{\mathrm{T}}(\Delta R < 0.4)/p_{\mathrm{T}}(\mu) < 0.1$

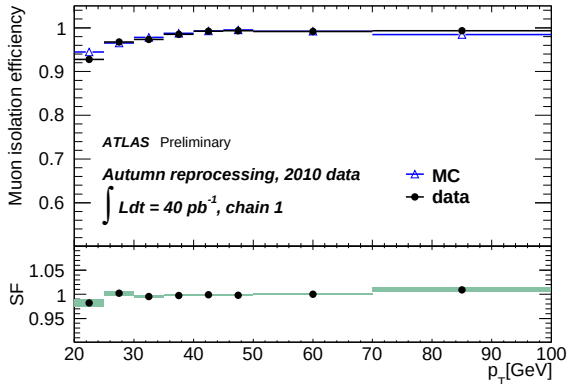


(e) Track isol. eff. for $\sum p_{\mathrm{T}}(\Delta R < 0.3)/p_{\mathrm{T}}(\mu) < 0.1$

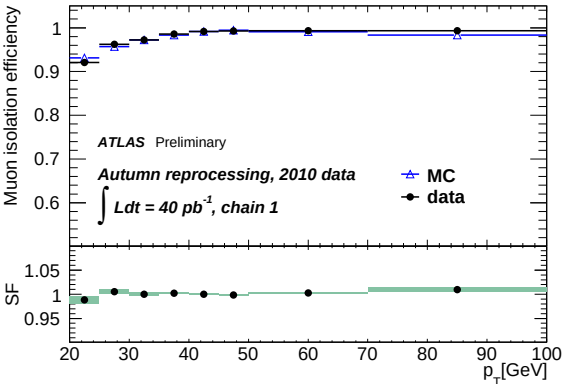


(f) Calorimeter isol. eff. for $E_{\mathrm{T}}(\Delta R < 0.3)/p_{\mathrm{T}}(\mu) < 0.1$

Figure 10: Muon isolation efficiency in $Z \rightarrow \mu^{+}\mu^{-}$ events for different isolation requirements. The Monte-Carlo prediction includes $Z$ signal and background processes.